PERGAMON

Scripta mater. 44 (2001) 1431–1435

Scripta MATERIALIA

www.elsevier.com/locate/scriptamat

OPTIMIZATION OF MAGNETIC PROPERTIES OF NANOSTRUCTURED Nd-Fe-B: APPROACHING IDEAL STONER-WOHLFARTH BEHAVIOUR

E. Girt[1,2], K.M. Krishnan[1] and G. Thomas[1,2]

[1]Material Science Division, Lawrence Berkeley National Laboratory, University of California, Berkeley, California 94720, USA [2]Department of Material Science and Mineral Engineering, University of California, Berkeley, California 94720, USA

(Received August 21, 2000)
(Accepted in revised form December 27, 2000)

Abstract—By appropriate annealing of rapidly quenched $Nd_\delta Fe_{13.1}B$ ($2.05<\delta<147.6$) the amount and microstructure of the $Nd_2Fe_{14}B$ grains in the Nd-rich matrix were systematically controlled and correlated with coercivity, $\mu_0 H_c$. For optimally annealed $Nd_\delta Fe_{13.1}B$ an increase in Nd concentration enhances $\mu_0 H_c$ of the $Nd_2Fe_{14}B$ grains (from 1.2 T in $Nd_{2.05}Fe_{13.1}B$ to 2.75 T in $Nd_{147.6}Fe_{13.1}B$ at 290 K) and promotes the growth of the $Nd_2Fe_{14}B$ grains elongated in shape. The largest observed coercivity, $H_c \sim 2.75$ T is over 80% of the theoretical limit expected for Stoner-Wohlfarth coherent rotation behavior including demagnetization effects.

Introduction

In theory, the nucleation field of randomly-oriented, non-interacting, single domain magnetic particles with $K_1 \gg K_2$ can be calculated as $\mu_0 H_N{}^{min} = 0.5(2K_1/M_s - NM_s)$ if the magnetic moments of these particles coherently rotate in the applied field [1]. Here K_1 and K_2 are the magnetocrystalline anisotropy constants, M_s is the spontaneous magnetization and N is the demagnetization factor. However, experimentally obtained values of the coercive field are at least two times smaller than the theoretically predicted values. The main reason for this discrepancy is that the coercive field in magnetic materials reflects both intrinsic magnetic properties and the microstructure of the material. Thus, only in materials with optimal microstructure, i.e., with non-interacting single domain magnetic particles, one might expect to approach the theoretical predicted values. Moreover, magnetic particle with a large enough K_1 are desired to insure coherent rotation of their magnetic moments.

Nd-Fe-B represents an ideal system because it is possible to form the high anisotropy $Nd_2Fe_{14}B$ grains in a non-magnetic matrix over a wide range of compositions as shown in the ternary Nd-Fe-B diagram, Bushow et. al. [2] (Fig. 1). The ternary diagram was obtained analyzing melt spun Nd-Fe-B samples thermally annealed below 1173 K (973 K for Nd-rich corner). Previously, systematic work has been done on the rapidly quenched Nd-Fe-B samples with compositions along the tie-line connecting the $Nd_2Fe_{14}B$ and $Nd_{1.1}Fe_4B_4$ phases [3]. Unfortunately, in this compositional region the soft magnetic Fe and Fe-B phases may precipitate during annealing introducing centers for domain wall nucleation that will directly reduce coercivity. For this reason we prepared a series of melt-spun samples along the tie-line connecting $Nd_2Fe_{14}B$ and pure Nd. As shown [4] there is a wide range of compositions around the tie-line where combination between the $Nd_2Fe_{14}B$ phase and Nd-rich paramagnetic phases can be formed by annealing rapidly quenched samples. The motivation was to obtain randomly oriented, single

1359-6462/01/$–see front matter.
PII: S1359-6462(01)00936-8

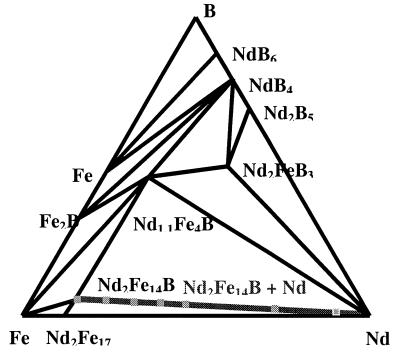

Figure 1. Ternary phase diagram of Nd-Fe-B at 1173 K (973 K for Nd rich corner). Crystalline phases observed after crystallization of amorphous Nd-Fe-B alloys. After Bushow et. al [2].

domain, $Nd_2Fe_{14}B$ particles embedded in a non-magnetic Nd matrix. By systematically changing the amount of the non-magnetic Nd matrix, the effect of the interaction on coercivity between $Nd_2Fe_{14}B$ was also investigated.

The change in the composition will have an effect on the microstructure and therefore on the magnetic properties of the Nd-Fe-B samples. Thus, in this paper we will also put an emphasis on the microstructural investigation of Nd-Fe-B using electron microscopy.

Experimental Techniques

The $Nd_\delta Fe_{13.1}B$ ($2.05 \leq \delta \leq 147.6$) alloys, prepared by arc-melting, were melt-spun in an argon atmosphere using a Cu wheel with a surface speed of 35 m/s. The as-quenched and annealed ribbons were characterized by differential scanning calorimetry (DSC), X-ray and thermomagnetic analysis (TMA) [5,6]. Results show that by changing the Nd concentration the ratio between the $Nd_2Fe_{14}B$ and Nd-rich can be systematically controlled in optimally annealed $Nd_\delta Fe_{13.1}B$ [5,6]. The magnetic measurements are performed with a SQUID magnetometer at 290 K with a maximum external field, $\mu_0 H_{ext} = 5.5$ T. In order to ensure a random crystallographic orientation of the $Nd_2Fe_{l4}B$ grains in the $Nd_\delta Fe_{l3.1}B$ ribbons, coercivity was measured in both ribbon and powdered ribbon (with particle sizes below 50 μm) samples. The details of the powder sample preparation and analyses of the SQUID measurements have been previously presented [5]. The M(H) loop of $Nd_\delta Fe_{13.1}B$ (except for $Nd_{2.05}Fe_{13.1}B$) contains contributions from the ferromagnetic $Nd_2Fe_{14}B$ and paramagnetic Nd-rich phases. The Nd-rich phase consists of mainly α-Nd and a few percent γ-Nd so it was assumed that α-Nd correctly accounts for the paramagnetic contribution in $Nd_\delta Fe_{13.1}B$. Microstructural analysis of $Nd_\delta Fe_{13.1}B$ was carried out by conventional transmission electron microscopy (TEM) and energy-filtered imaging using inner-shell ionization edges in electron energy-loss spectroscopy. The later was done on $Nd_\delta Fe_{13.1}B$ ($\delta = 38.1, 147.6$) by selecting energy windows around the Nd $M_{4,5}$ edge for mapping Nd and energy windows around the Fe $L_{2,3}$ edge for mapping Fe. For each map, one energy window was positioned at the onset of the characteristic edge to obtain the signal due to the energy-loss of the transmitted electrons (post-edge image) and two energy windows before the edge to extrapolate the background below the ionization edge (pre-edge 1 and pre-edge 2 images) [7]. The widths of the energy windows were 20 eV for Fe and 30 eV for Nd. The Nd and Fe jump ratio images, obtained by dividing the post-edge by the pre-edge 2 image [7]. The $Nd_2Fe_{14}B$ grains are dark in the Nd map and bright in the Fe map.

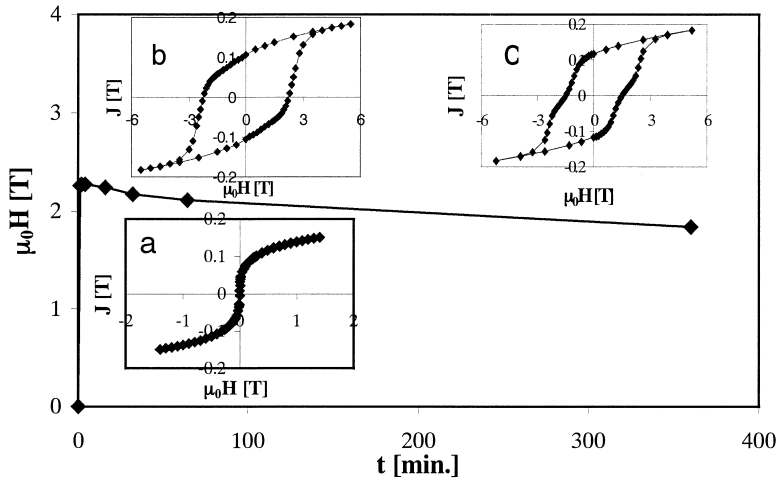

Figure 2. Coercive field $\mu_0 H_c$ as a function of the annealing time for $Nd_{38.1}Fe_{13.1}B$ annealed at 873 K. M-H loops for a) as quenched, b) annealed for 2 min., and c) annealed six hours, $Nd_{38.1}Fe_{13.1}B$ ribbons.

Results and Discussions

The annealing is crucial to obtain a large coercivity of the rapidly quenched $Nd_\delta Fe_{13.1}B$ samples. Fig. 2 shows the dependence of the coercive field, $\mu_0 H_c$, on the annealing time for $Nd_{38.1}Fe_{13.1}B$. The corresponding microstructure of these samples is presented in Fig. 3. The M(H) loop shows that the as-quenched $Nd_{38.1}Fe_{13.1}B$ exhibits both soft magnetic behavior (Fig. 2a). The selected area diffraction and bright field images, Fig. 3a, show that the as-quenched sample has both amorphous (diffuse ring pattern) and nano-crystalline structure (Fig. 3a). The largest $\mu_0 H_c$ was obtained after annealing for 2

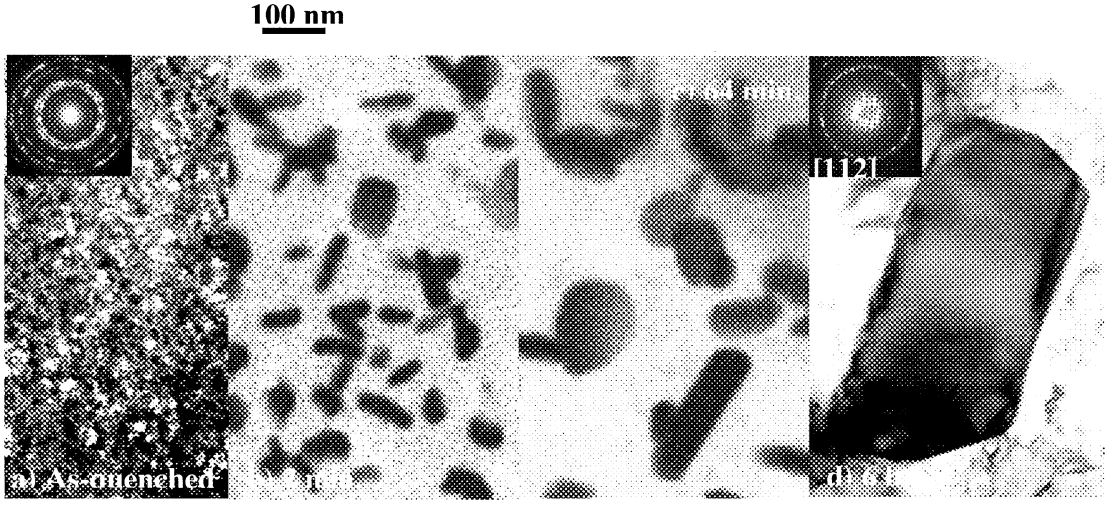

Figure 3. The grain size of $Nd_2Fe_{14}B$ as a function of the annealing time in $Nd_{38.1}Fe_{13.1}B$ annealed at 873 K. Fig. 3a) bright field image of as quenched $Nd_{38.1}Fe_{13.1}B$ with selected area diffraction pattern, Fig. 3b) and 3c) energy filtered images of $Nd_{38.1}Fe_{13.1}B$ annealed at 2 and 64 min. respectively and 3d) bright field images of $Nd_{38.1}Fe_{13.1}B$ annealed at 6 hours with [112] selected area diffraction pattern of $Nd_2Fe_{14}B$.

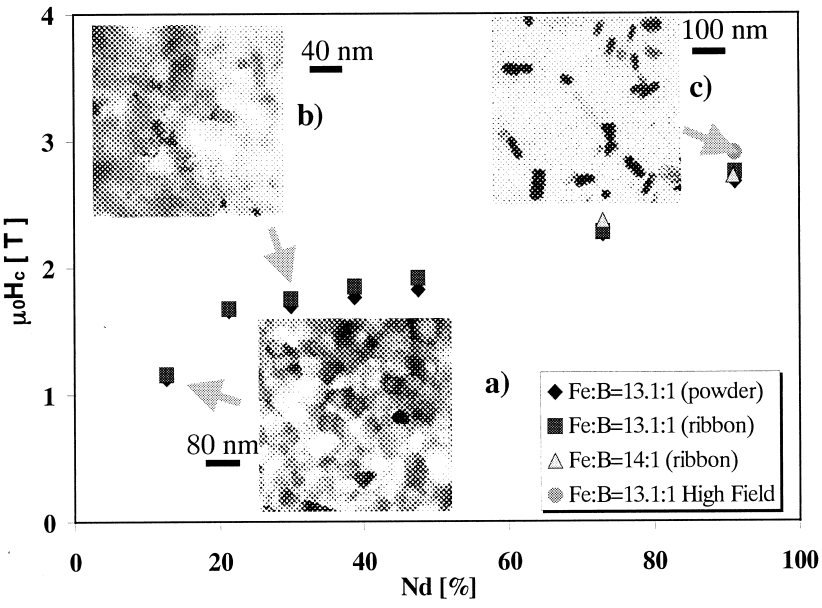

Figure 4. The coercivity of the $Nd_2Fe_{14}B$ phase as a function of Nd concentration. The error in the measurements is smaller than the symbols. Figures 4a) and 4b) represent bright field images of $Nd_\delta Fe_{13.1}B$ (δ = 2.05, 6) and figure 4c) energy filtered image of $Nd_{147.6}Fe_{13.1}B$.

min. at 873 K (Fig. 2b). This sample contains plate-like $Nd_2Fe_{14}B$ grains, 100 nm long, embedded in the Nd-rich matrix. The size of the $Nd_2Fe_{14}B$ grains is close to the single magnetic domain size (~100 nm) that is the optimal microstructure for obtaining a large $\mu_0 H_c$. Further annealing decreases $\mu_0 H_c$ due to the formation of grains significantly larger than that for single magnetic domains.

For example, for samples annealed for six hours $\mu_0 H_c$ decreases by about 30% (Fig. 2c) and the $Nd_2Fe_{14}B$ grains are larger than 0.5 μm (Fig. 3d). As shown the microstructure of $Nd_\delta Fe_{13.1}B$ is very sensitive to the annealing conditions. Moreover, DSC measurements show that the crystallization temperature of the $Nd_2Fe_{14}B$ phase decreases with an increase of the Nd concentration for $\delta \leq 38.1$ in $Nd_\delta Fe_{13.1}B$. Thus, to obtain the optimal microstructure both annealing time and temperature are adjusted separately for each composition. The optimal annealing conditions for $Nd_{2.05}Fe_{13.1}B$, $Nd_\delta Fe_{13.1}B$ (δ = 3.8, 6, 8.9, 12.7) and $Nd_\delta Fe_{13.1}B$ (δ = 38.1, 147.6) ribbons were found to be 4 min. at 923 K, 2 min. at 873 K and 4 min. at 823 K, respectively.

The M(H) measurements show that the coercivity of the $Nd_2Fe_{14}B$ phase in $Nd_\delta Fe_{13.1}B$ (Fig. 4) increases with an increase in the Nd concentration from 1.2 ± 0.03 T for $Nd_{2.05}Fe_{13.1}B$ to 2.75 ± 0.03 T for $Nd_{147.6}Fe_{13.1}B$. The error bars were estimated from measuring four different ribbon samples with the same composition. Fig. 4 shows that the discrepancy between the values of coercivity obtained for the ribbon and powder samples is small, confirming the random orientation of the $Nd_2Fe_{14}B$ grains in the ribbons. The microstructure of $Nd_\delta Fe_{13.1}B$ also changes with the Nd concentration. The bright field image (Fig. 4) shows that the $Nd_{2.05}Fe_{13.1}B$ sample contains uniform distribution of the polyhedral $Nd_2Fe_{14}B$ grains approximately 40 nm in size. The higher Nd concentration promotes the growth of the $Nd_2Fe_{14}B$ grains elongated in shape as can be seen from the bright field image of $Nd_6Fe_{13.1}B$ and the energy-filtered image of $Nd_{147.6}Fe_{13.1}B$ (Fig. 4). Detailed analyses of $Nd_{147.6}Fe_{13.1}B$ [5] confirms that the $Nd_2Fe_{14}B$ grains are platelets with an average size of $a \times b \times c = 100 \times 40 \times 25$ nm. The high resolution lattice image of a representative $Nd_2Fe_{14}B$ grain in optimally annealed $Nd_{147.6}Fe_{13.1}B$ shows that the shortest side of the plate is along the crystallographic c-axis [5].

For such randomly oriented, non-interacting, single domain, magnetic particles, the coercivity calculated from the Stoner-Wohlfarth model [1] should be equal to about half of the nucleation field $\mu_0 H_c \approx 0.5\ \mu_0 H_N$. Since, in $Nd_2Fe_{14}B$ at 290 K, $K_1 > 4K_2$, the coercivity can be calculated [8] as, $\mu_0 H_c = 0.5\ \mu_0 H_N = (K_1 + K_2)/M_s - 0.5(N_\parallel - N_\perp)M_s$. $N_\parallel$ and $N_\perp$ are the demagnetization factors parallel and perpendicular to the c-axis of the $Nd_2Fe_{14}B$ platelets and can be determined assuming that the $Nd_2Fe_{14}B$ grains in $Nd_{147.6}Fe_{13.1}B$ are ellipsoids with axes $a = 20$ nm, $b = 50$ nm and $c = 12.5$ nm [9]. K_1, K_2, and M_s values of $Nd_2Fe_{14}B$ are taken from the literature [10]. It follows that the coercivity of the $Nd_2Fe_{14}B$ grains in $Nd_{147.6}Fe_{13.1}B$ should be equal to $\mu_0 H_c = 3.33$ T. Thus the measured coercivity of the $Nd_2Fe_{14}B$ grains in $Nd_{147.6}Fe_{13.1}B$ is about 83% of the theoretical value of coercivity obtained from the Stoner-Wohlfarth model for an assembly of randomly oriented, non-interacting, single domain particles.

Conclusions

By appropriate annealing of rapidly quenched $Nd_\delta Fe_{13.1}B$ ($2.05 < \delta < 147.6$) the amount and microstructure of the $Nd_2Fe_{14}B$ grains in the Nd-rich matrix were systematically controlled. For optimally annealed $Nd_\delta Fe_{13.1}B$ an increase in Nd concentration enhances $\mu_0 H_c$ of the $Nd_2Fe_{14}B$ grains (from 1.2 T in $Nd_{2.05}Fe_{13.1}B$ to 2.75 T in $Nd_{147.6}Fe_{13.1}B$ at 290 K) and promotes the growth of the $Nd_2Fe_{14}B$ grains elongated in shape. The largest observed coercivity, $H_c \sim 2.75$ T is over 80% of the theoretical limit expected for Stoner-Wohlfarth coherent rotation behavior including demagnetization effects.

References

1. E. C. Stoner and E. P. Wohlfarth, Phil. Trans. Roy. Soc. London. A240, 599 (1948).
2. K. H. J. Buschow, D. B. de Mooij, and H. M. Van Noort, J. Less. Common Met. 115, 357 (1986).
3. V. Villas-Boas, F. P. Missell, G. Schneider, Q. Lu, and D. Givord, Solid State Commun. 74, 683 (1990).
4. E. Girt, K. M. Krishnan, G. Thomas, C. J. Echer, and Z. Altounian, Proceedings of the MRS Meeting, San Francisco, April 5–9, 1999, in press.
5. E. Girt, K. M. Krishnan, G. Thomas, and Z. Altounian, Appl. Phys. Lett. 76, 1746 (2000).
6. E. Girt, K. M. Krishnan, G. Thomas, E. Girt, and Z. Altounian, J. Magn. Magn. Mater. in press.
7. F. Hoffer, P. Warbichler, W. Grogger, and G. Kothleitner, Microsc. Anal. November, 11 (1995).
8. G. Martinek and H. Kronmüller, J. Magn. Magn. Mater. 86, 177 (1990).
9. J. A. Osbon, Phys. Rev. B. 67, 351 (1945).
10. S. Hock, H. Kronmüller, Proceedings of the 5th International Symposium of Magnetic Anisotropy and Coercivity in Rare Earth-Transition Metal Alloys, Bad Soden, Germany, 275 (1987).